ELSEVIER

J. Non-Newtonian Fluid Mech. 126 (2005) 47–61

Journal of Non-Newtonian Fluid Mechanics

www.elsevier.com/locate/jnnfm

The effect of die exit curvature, die surface roughness and a fluoropolymer additive on sharkskin extrusion instabilities in polyethylene processing

D.R. Arda, M.R. Mackley *

Department of Chemical Engineering, University of Cambridge, New Museums Site, Pembroke Street, Cambridge CB2 3RA, UK

Received 3 March 2004; received in revised form 24 September 2004; accepted 20 December 2004

Abstract

This paper reports experimental observations and numerical simulations relating to sharkskin extrusion instabilities for two different types of polyethylene, a metallocene high-density polyethylene (HDPE) and a linear low-density polyethylene (LLDPE). Experimental results are presented for both the effect of die exit curvature and die surface roughness for slit die geometry. Matching polyflow numerical simulations are also reported and are shown to be qualitatively consistent with experimental observations. The onset of the sharkskin instability is correlated with the magnitude of the stress concentration at the die exit, and is found to be sensitive to both the melt/wall separation point for a curved exit die, and the level of partial slip at the die wall. Additional observations on the effect of a fluoropolymer additive also support the sensitivity of the sharkskin instability to partial slip at the wall.

Keywords: Sharkskin; Instability; Polyethylene; Extrusion; Curved exit dies; Die surface roughness; Fluoropolymer; Slip

1. Introduction

This paper is concerned with sharkskin extrusion instabilities for polyethylene and investigates ways of minimising its occurrence. Sharkskin is generally described as fine-scale, high frequency, small-amplitude distortions or surface roughness (see, for example [1–3]). The instability can appear at high shear stresses for certain polymers and can hinder the optical and mechanical properties of the polymer product, thereby limiting the rate of polymer production. The subject is of both scientific and commercial interest and has been extensively reviewed by [1–6].

1.1. Sharkskin origin

Although there have been numerous studies on sharkskin instabilities over the past 50 years, there is still no clear consensus as to the exact mechanism that causes its onset. It is generally accepted that, whatever may be happening within the die, overriding experimental evidence shows that the sharkskin instability originates at the die exit [7,8]. A growing number of researchers believe that the origin of sharkskin is related to local stress concentrations in the melt near the die exit [9–12]. However, the mechanism by which the stress concentrations actually cause sharkskin is still a subject of debate. A number of proposed mechanisms are outlined below.

1.1.1. Rupture mechanisms

Cogswell [9] proposed that the polymer extrudate fractures at the die exit due to an abrupt change in the flow boundary conditions. He explained that downstream of the die exit, the surface layer of the melt accelerates from rest to the average extrusion velocity. The acceleration causes a stretching flow, producing tensile stresses higher than the tensile strength that the material can withstand, giving rise to cracking of the surface at the exit, which in turn leads to a momentary relaxation of flow conditions near the edge. This continues in a cyclic manner, giving rise to the sharkskin phenomena. This explanation is consistent with the visual observations made just at the die exit by El Kissi and Piau

* Corresponding author. Tel.: +44 1223 334777; fax: +44 1223 334796.
E-mail address: malcolm_mackley@cheng.cam.ac.uk (M.R. Mackley).

0377-0257/$ – see front matter © 2005 Elsevier B.V. All rights reserved.
doi:10.1016/j.jnnfm.2004.12.005

[11], who reported the appearance of cracks perpendicular to the flow direction. In addition, Rutgers and Mackley [12] proposed that a rupture mechanism could explain the correlation between sharkskin and melt strength. The mechanism is supported by numerous authors [8–15].

Legrand and Piau [16] and Inn et al. [15] attributed sharkskin to a layer of polymer melt close to the die wall sticking to the rim of the die exit as it is extruded with die swell. The outer layers of the melt stick to the exit rim and the inner layers move with the extrudate. They claim that the surface fracture begins in a form of peeling. After the ridge has grown to a certain size, it is torn from the die exit and moved forward with the whole extrudate, and immediately a new ridge starts at the rim of the die exit. In support of this model, Inn et al. found that dies with a sharp exit induce uniform and well-defined sharkskin ridges, because the surface layer of the melt can stick to only one fixed position on the die edge. The extrudates from rounded exit dies, however, have non-uniform ridges, because the surface layers appear to stick arbitrarily on the surface of the exit [15].

1.1.2. Slip mechanisms

In 1986, Ramamurthy [17] carried out measurements using a technique outlined by Mooney [18] and demonstrated that for certain polymers, partial slip occurs at the die wall above the critical shear stress for sharkskin. He then argued that the several categories of extrudate distortion are part of a continuum behaviour associated with the occurrence of wall slip, and that the first onset of sharkskin occurs with a failure of adhesion at the melt/die wall interface along the die land. Kalika and Denn [19] also showed evidence that the onset of sharkskin and the apparent curvature of the flow curve for a linear low-density polyethylene (LLDPE), are both caused by partial slip of the melt at the die surface. This mechanism, which proposes that sharkskin is enhanced with slip, appears to be inconsistent with results of Migler et al. [20] and Yang et al. [21], who show that the presence of a thin layer of fluoropolymer at the melt/die wall interface enhances slip but suppresses sharkskin, rather than causes its onset. Migler et al. used optical velocimetry to show that sharkskin can occur under a variety of melt/wall boundary conditions: stick, slip or oscillating stick-slip [20].

Wang and Drda [22] explained the sharkskin distortions in terms of melt/wall interfacial interactions at a molecular level. Their proposed mechanism states that sharkskin occurs because of a local conformational transition at the die wall exit, where the adsorbed chains entrap a layer of interfacial chains. This layer oscillates between entanglement and disentanglement states due to a reversible coil-stretch transition. The corresponding oscillation of the exit wall boundary condition leads to cycles of local stress relaxation and growth, and to periodic perturbation of the extrudate swell in the form of sharkskin-like surface roughening on the extrudate. In support of this mechanism, sharkskin dynamics of linear low-density polyethylene has been found to correlate precisely with molecular chain relaxation dynamics [22–24].

Molenaar and Koopmans [25] proposed a local mechanism of stick-slip or relaxation oscillations in a thin peripheral layer near the die exit, similar to the oscillating defect observed at higher stresses. They modelled melt flow instabilities in terms of cyclic relaxation oscillations, during which potential energy is successively stored and relaxed, and found that above a critical wall shear stress, the increase in the flow curve becomes non-monotonic and successive stick-slip oscillations develop within a localised area at the die exit.

An alternative local stick-slip mechanism for LLDPE was proposed by Dhori et al. [26–28], who attributed stick-slip to the dewetting-wetting process between the melt and the die wall at the die exit corner. They asserted that the dewetting was the result of exceeding a critical surface elastic energy, while the rewetting was the result of a relaxation process. According to this mechanism, sharkskin is suppressed by local die exit coatings such as PTFE, because the coating forms a relatively low energy solid surface that the polymer cannot rewet [28].

Joseph and Liu [29], on the other hand, suggested that the asymmetric aspect of sharkskin could result from a thin lubricating layer (which, for example, could be a molecular mass fraction of the polymer) with a steep wave front. Joseph [30] argued that this lubricating layer allows the polymer melt to slip along the die wall, creating sharp steep (sharkskin) waves, such as those that appear on flows of heavy oil lubricated by water.

Both the melt fracture mechanism, and the mechanism that proposes local stick-slip of the melt at the die exit, are consistent with observations of local oscillations of birefringence or stress fringes at the die exit. Legrand and Piau [16] observed that the onset of these stress oscillations coincided with the onset of the sharkskin instability for PDMS. They viewed and recorded periodic cracking of the melt at the die exit, and found that the period of the stress oscillation matched with the sharkskin crack formation period. Barone and Wang [31] observed birefringence oscillations during the sharkskin regime of polybutadiene and also found that the period of the oscillations agreed with the period of the ridges produced on the sharkskin extrudate. They explain that the oscillation occurs because of the unstable slip boundary condition at the die exit [31].

1.1.3. Other mechanisms

Tremblay [32] suggested that negative pressures close to the die exit could induce the formation of vacuum spaces by cavitation, the coalescence of which would then produce sharkskin instabilities.

1.2. Current sharkskin minimisation methods

1.2.1. Additives

The most common method of eliminating sharkskin, or postponing it to higher flow rates, has been the use of

polymer processing additives (PPA), such as a fluoropolymer. When a fluoropolymer is blended into polyethylene in an extruder, it has been found that the fluoropolymer becomes dispersed in the polyethylene in the form of spherical droplets, 0.1–0.5 μm in diameter [33]. The fluoropolymer was found to be incompatible with the polyethylene, causing a uniform, continuous coating of strongly adhered fluoropolymer, of the order of 1 μm thick, which was deposited during extrusion on the extruder screw, barrel and die surfaces [34]. No fluoropolymer was found on the surface of the polyethylene after extrusion, suggesting that a sharp interface existed between the fluoropolymer coating and the polyethylene melt during extrusion. It appeared that fluoropolymers act as processing aids by forming a thin uniform coating on die surfaces, which provides a sharp, low energy interface over which, at sufficiently high shear stress, the polyethylene can slip [34]. It has also been discovered that fluoropolymer can act either as an adhesion promoter or as a slip promoter, depending on the coating method [35]. If the coating method results in a porous fluoropolymer coating, this enhances melt/die wall adhesion, whereas if the method results in a non-porous coating, slip is promoted.

A more recent processing additive that was found to significantly delay the onset of sharkskin is boron nitride (BN) [36]. The authors found that the addition of a composition of fine particles of BN eliminated sharkskin as well as postponed the critical shear rate for the onset of gross distortion to significantly higher values [37].

1.2.2. Coatings

Coating the die wall with a low surface energy material such as PTFE has been found to eliminate, or at least considerably delay the sharkskin instability [17,38,39]. While Ramamurthy [17] attributed this result to increased adhesion of the melt to the die wall, Piau et al. [38] proposed that the coating material promotes slip at the die wall, thereby reducing the exit stresses. Recently, Kulikov and Hornung [40] found that coating the die land with a rubber compound produced defect-free extrusion, for flow rates 10 times higher than those in Teflon dies. Coatings of PTFE or rubber that are localised just at the exit of the die wall, have also been found to be effective at delaying the onset of sharkskin, though to a lesser extent than a coating along the whole die surface [38,40].

This paper systematically explores the effect that die exit curvature, die wall surface roughness and a fluoropolymer additive have on sharkskin instabilities. Both experimental results and matching numerical simulations are presented. Two distinctly different types of polyethylene are examined, namely a commercial grade of LLDPE where sharkskin instabilities have been observed previously and a developmental grade metallocene high-density polyethylene (HDPE) that shows pronounced extrusion instabilities.

2. Experimental

2.1. Materials

The two materials studied were Dowlex NG5056E linear low-density polyethylene supplied by Dow Benelux B.V. and a metallocene development grade high-density polyethylene homopolymer supplied by Repsol YPF. The HDPE was supplied both without and with a fluoropolymer additive supplied by Dyneon GmbH. The LLDPE was chosen as a reference comparison to the HDPE. Material properties of the polymers are given in Table 1 and the linear viscoelastic spectrum parameters and a non-linear Wagner damping factor obtained from rheological characterisation are given in Table 2 (see [41] for details on how this data was obtained). The Dowlex LLDPE was a heterogeneous blend of linear polyethylene and polyethylene chains with varying numbers of octene-1 branches. Its main application is in blown film extrusion. The fluoropolymer was a linear random terpolymer of tetrafluoroethylene (40 mol%), hexafluoropropylene (10 mol%) and vinyldenfluoride (50 mol%). Its main application area is within the automotive industry where it is used in hose applications under the bonnet.

Preparation of the fluoropolymer as a polymer-processing additive to the HDPE was carried out in the following way. A master-batch of 30,000 ppm (3%, w/w) fluoropolymer/HDPE was supplied by Dyneon. This master-batch was diluted to the final recommended concentration of 1500 ppm (0.15%, w/w) by shaking and stirring the mixture with a large spoon in a container for 5 min to ensure homogeneity. In order to aid the deposition of additive on the internal walls of the extruder and die, the master-batch was extruded through the system until a reduction in pressure drop was observed. The 1500 ppm batch was then extruded subsequently.

2.2. Extrusion apparatus

Extrusion experiments were carried out using a 25 mm single screw extruder equipped with a melt gear pump designed to control the flow rate and the extruder screw speed through a pressure feedback system (see [41] for further details). The dies were held in a stainless steel flow cell that allowed interchangeable die inserts. The polymer extrudate was hauled off vertically using a haul off machine with controllable rotational speed.

The flow cell was designed to accommodate optical windows, which would enable the set-up of an optical line-up for flow birefringence measurements. A mercury lamp was used with a 546 nm wavelength (green) filter to provide monochromatic light. The flow cell was placed between a polariser, oriented at 45° with respect to the principle flow direction, and an analyser, oriented at −45°. The transmitted picture of dark and light bands were captured by a CCD camera and recorded onto video.

The features of the various die inserts used in the experiments described in this paper are summarised in Table 3. All

Table 1
Physical properties of the LLDPE, HDPE and the fluoropolymer

Material	Dowlex LLDPE NG5056E	HDPE 0017 ZSK	Fluoropolymer THV220G
Supplier	Dow Benelux B.V	Repsol YPF	Dyneon GmbH
Density (g/cm^3), RTP	0.9195	0.9521	1.937
Mn (g/mol)	54,800	53,400	46,900
Mw (g/mol)	113,000	122,900	75,000
Mw/Mn	2.1	2.3	1.6

Table 2
Spectrum coefficients $\{g_i, \lambda_i\}$ and damping factors, k for the LLDPE, HDPE and the fluoropolymer

LLDPE		HDPE		FP	
λ_i (s)	g_i (Pa)	λ_i (s)	g_i (Pa)	λ_i (s)	g_i (Pa)
2.09×10^{-3}	2.43×10^{5}	2.00×10^{-3}	3.38×10^{5}	2.11×10^{-3}	1.88×10^{5}
9.51×10^{-3}	1.44×10^{5}	9.38×10^{-3}	2.28×10^{5}	9.27×10^{-3}	2.04×10^{5}
4.32×10^{-2}	5.34×10^{4}	4.40×10^{-2}	7.05×10^{4}	4.07×10^{-2}	1.17×10^{5}
1.96×10^{-1}	1.25×10^{4}	2.06×10^{-1}	1.06×10^{4}	1.79×10^{-1}	3.30×10^{4}
8.90×10^{-1}	2.08×10^{3}	9.69×10^{-1}	1.30×10^{3}	7.86×10^{-1}	5.36×10^{3}
4.04×10^{0}	2.83×10^{2}	4.54×10^{0}	2.18×10^{2}	3.45×10^{0}	1.00×10^{3}
1.84×10^{1}	2.24×10^{1}	2.13×10^{1}	1.73×10^{1}	1.52×10^{1}	1.29×10^{2}
8.33×10^{1}	9.59×10^{-6}	1.00×10^{2}	1.37×10^{-5}	6.67×10^{1}	1.54×10^{1}
$k = 0.21 \pm 0.02$		$k = 0.23 \pm 0.04$		$k = 0.37 \pm 0.05$	

dies had curved entries, a parallel die length of approximately 8 mm, and die gaps of 1.2 mm and die depths of 15 mm. Dies A–C had identical surface roughness of 1.5 μm centre line average (CLA). The first die had a conventional 90° exit (die A); the others were radiused such that their exits are curved at 0.8 mm (die B) and 2 mm (die C), respectively.

Dies D–F had different surface roughness. Die D had a medium finish of 1.5 μm CLA, die E had a semi-polished finish of 0.7 μm CLA and die F had a technically polished finish of 0.05 μm CLA. The dies had curved exits of radius 0.8 mm similar to die B. The dies were assembled ensuring similar gap widths of 1.2 mm. The accuracy of the slit width was controlled by tightening the inserts with a feeler gauge in place, such that the feeler gauge could only just be removed without friction.

Flow rates in this paper are given in RPM, corresponding to the melt gear pump speed. Corresponding mass flow rates can be obtained using Fig. 1. Volumetric flow rates were calculated assuming a melt density of 760 kg/m^3.

The extrudates were examined using scanning electron microscope (SEM) and surface profilometry techniques. SEM was carried out using a Leica Stereoscan 430 scanning electron microscope. The profilometer was a contact roughness measurement technique that consisted of a stylus with a small tip that was automatically traversed along the surface to be examined. As the stylus moved up and down along the surface, a transducer (pick-up) converted this movement into a signal that was then exported to a processor that converted this into a number and a visual profile. A Talysurf six instrument was used with a standard diamond cone stylus with a cone angle of 90° and a tip radius of 2 μm. The pick-up used was a 112/2033-P3. Surface roughness values in this paper are given as Rq, defined as the root mean square roughness value of a profile.

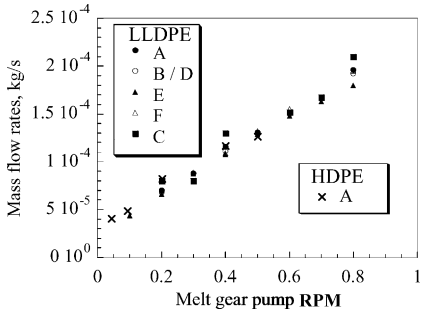

Fig. 1. Plot of mass flow rate vs. melt gear pump speed for extrusion of the LLDPE at 190 °C through dies A–F and for the HDPE at 190 °C through die A.

Table 3
Die exit and surface roughness features of the die inserts used in the experiments described in this paper

Features	Dies					
	A	B	C	D	E	F
Die exit	90°	0.8 mm rad	2 mm rad	0.8 mm rad	0.8 mm rad	0.8 mm rad
Surface roughness (μm CLA)	1.5	1.5	1.5	1.5	0.7	0.05

CLA, centre-line average.

3. Numerical simulation

Numerical simulations were carried out using the commercial finite element CFD package polyflow. Simulations used the KBKZ integral equation with the Wagner irreversible damping factor to predict principal stress differences (PSD) values in the melt flowing through the die (see for example [12]). Meshes were constructed with a 90° exit angle, a 0.8 mm radiused exit and a 2 mm radiused exit, corresponding to the dies used experimentally. In order to carry out simulations of the radiused exit dies, it was necessary to specify the separation points of the melt from the die. This was done using data from the matching experimental observations and meshes were generated with these experimentally obtained separation points. All meshes were designed with 30 μm × 30 μm size elements at the die wall at the die exit and are shown in Fig. 2. The parameters used in the numerical simulations were for LLDPE and HDPE at 190 °C and at a flow rate of 2.4×10^{-7} m^3/s. This was a typical high experimental extrusion flow rate within the sharkskin regime and corresponded to a wall shear stress of approximately 0.2 MPa.

The finite element formulation in polyflow used quadratic interpolation for velocities and linear interpolation for pressure. The boundary conditions assumed were a fully developed flow 25 mm upstream of the slit entrance before the curved entry region, with initially no slip at the die wall. The convergence criterion was set to 10^{-3}. A mesh sensitivity study investigated three meshes refined such that the elements immediately at the wall at the exit were 30 μm × 30 μm, 20 μm × 20 μm and 15 μm × 15 μm, respectively. The resulting streamlines and global stress contours were qualitatively compared and the pressure drops, velocities and stresses along the centreline and the PSD along streamlines close to the die wall were quantitatively compared. These were found to match across the three dies.

A difference in the solution between the three meshes with different exit element sizes only occurred in the element closest to the wall at the exit. This was the consequence of a mathematical singularity at the die exit [42,43]. It was found that the more refined the mesh, the higher the numerically predicted stress in the one node adjacent to the wall. However, in the present study, for the element sizes of 30 μm × 30 μm, 20 μm × 20 μm and 15 μm × 15 μm at the die wall at the exit, the exit PSD peaks were calculated outside the element nearest the wall, along streamlines 50 μm from the wall, and these values were found to agree to within 2%. It was, therefore concluded that mesh independence of the simulation was obtained outside the element immediately adjacent to the wall, which in this case was 30 μm for the coarsest mesh. The 2% agreement in the values of the PSD peaks was considered adequate and subsequent simulations were, therefore, carried out with meshes having exit element sizes 30 μm × 30 μm.

The mathematical singularity occurs at the corner of the die wall. Tracking along a streamline 50 μm from the die wall, polyflow predicted that the maximum PSD also occurred in line with the die wall corner. Since the corner of the die exit is the point of the abrupt change in boundary condition, as well as the point of maximum PSD, it would seem reasonable to expect that this is the point where sharkskin is initiated. Manifestation of the sharkskin characteristics would be expected to take place slightly downstream of the die exit, since it would take a finite time for the wave to propagate within the melt. Venet and Vergnes [44], however, used a finite element method incorporating the Phan-Thien and Tanner constitutive equation to predict the tensile or extensional stresses in the melt in the die exit region and found that the maximum extensional stress actually occurred slightly downstream of the die exit at the surface of the melt. They proposed that the actual rupture of the melt occurs at this position of maximum extensional stress, downstream of the die exit.

Quantitative matching of experimental and simulated stress birefringence and extrusion pressure drops for the experimental die geometries presented in this paper has not been made. However, a quantitative matching of extrusion pressure drop has been carried out for the same material LLDPE and at the same temperature of 190 °C for different die geometry and this is shown in Fig. 3.

4. Results and discussion

4.1. The effect of die exit curvature

4.1.1. Stress field

Flow birefringence images of LLDPE extruded through dies A–C, which had different die exit curvatures, are shown in Fig. 4. The images are for a lower flow rate than that where sharkskin occurs because the high flow rate images, where sharkskin does occur, are unclear due to the high number of fringes. The images show that in the parallel section of the die, the fringes and therefore the stresses are parallel to the die wall. An identical number of fringes are observed in each die, showing that the stresses in the parallel section of the dies are of equal magnitude. The local stress concentrations at the die exit are difficult to resolve; however, it is possible to see that with curvature of the die exit, separation of the melt from the die no longer occurs at the smallest gap width and the separation is delayed. The separation is more delayed for die C than die B. Qualitatively, the stress concentrations appear to be lower for the curved exit dies.

4.1.2. Extrudate surface

SEM images of the extrudate surfaces from dies A–C at 0.6 rpm are shown in Fig. 5. The images show the results of extrusion at moderately high flow rates in a flow regime where sharkskin occurs. It was observed that while there was not a significant reduction in sharkskin from die A to die B, there was a definite reduction in sharkskin from die A to die C. The onset of the sharkskin instability, as observed visually from SEM, was as follows: 0.4 rpm for die A (wall shear stress $\tau_w = 0.14$ MPa), 0.4 rpm for die B ($\tau_w = 0.16$ MPa) and 0.6 rpm for die C ($\tau_w = 0.17$ MPa). Fig. 5 also shows sur-

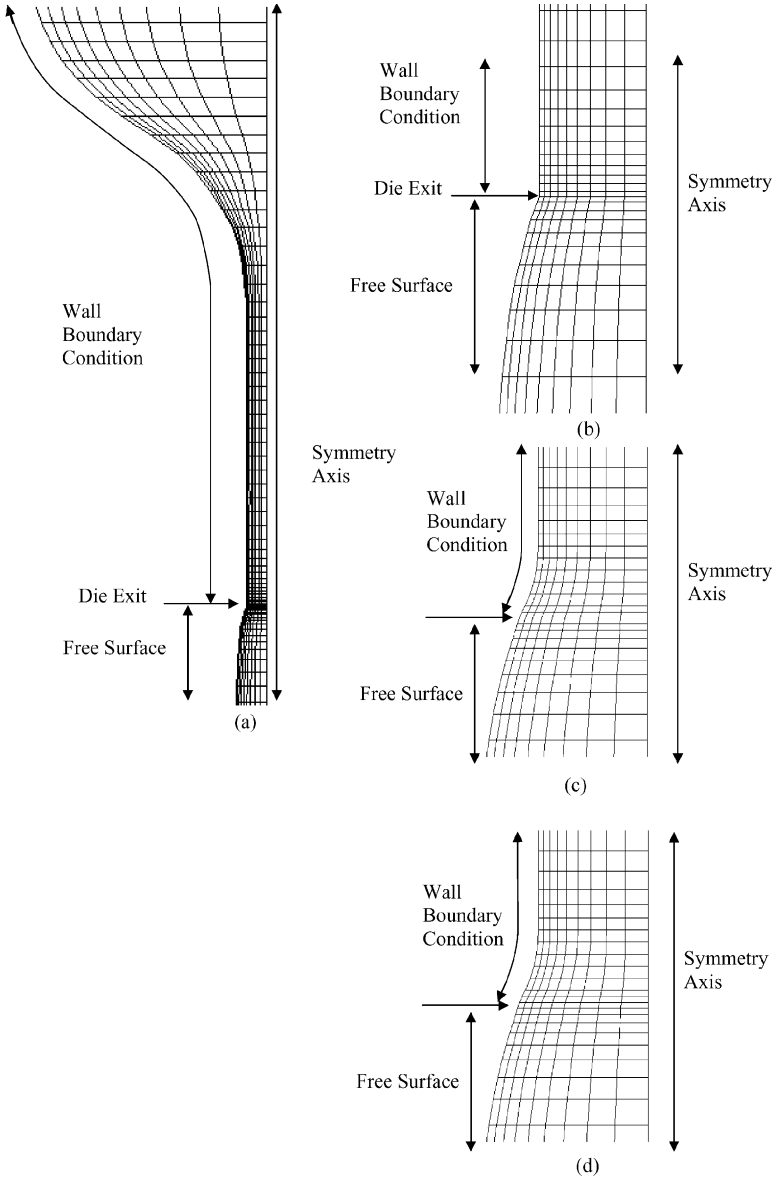

Fig. 2. Meshes used to simulate dies (a) mesh for die A (900 elements), (b) close-up of die A exit, (c) close-up of die B (918 elements) exit and (d) close-up of die C (954 elements) exit.

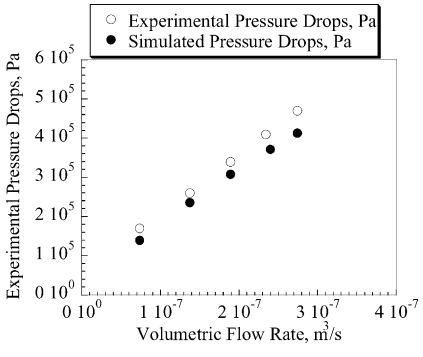

Fig. 3. A comparison of simulated and experimental extrusion pressure drops across a square entry die for different flow rates for Dowlex LLDPE at 190 °C.

face profilometry for the samples that was carried out in order to quantify the surface roughness results. Rq values (the root mean square roughness) were calculated and are also shown with the roughness profiles. The results show that the scale of the roughness is relatively small (of the order of 1 μm), and the pattern of roughness is very periodic. A reduction in sharkskin magnitude of 13% is observed from die A to B and a 45% reduction is observed from die A to C.

4.1.3. Comparison of pressure drop

A comparison of the extrusion pressure drops obtained through each die is shown in Fig. 6. While it was expected that die A would have the highest pressure drop,

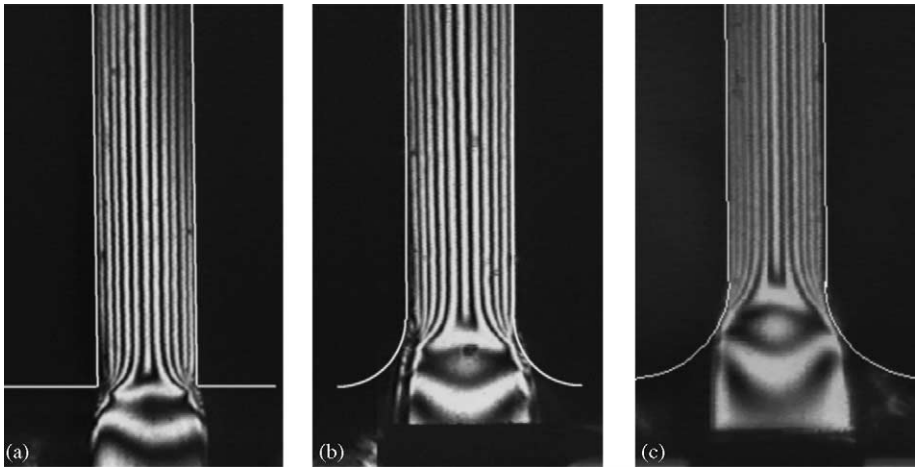

Fig. 4. Flow birefringence images for the LLDPE extruded at 0.05 rpm and 190 °C through dies (a) A, (b) B and (c) C.

the greatest pressure drop was actually found for die B. However, the differences between pressure drops for the three dies are small in comparison to the experimental error of 10%, which appears to be high as it takes into account the pressure drop variation that occurred with the unsteadiness of the extrusion temperature and also depending on whether the flow rates were being increased for the first time or after they had been increased and decreased a few times.

4.1.4. Stability of the melt/wall separation point

Extrudates from the curved exit dies appeared to emerge in a waveform, swaying from side to side with a time period of the order of seconds. This effect appeared to be more enhanced for the die with the most highly curved exit (die C) and was not observed for the die with the conventional 90° exit (die A). An explanation for this effect could be the instability of the separation point between the melt and the die wall at the exit. While for 90° exit dies, the melt separates

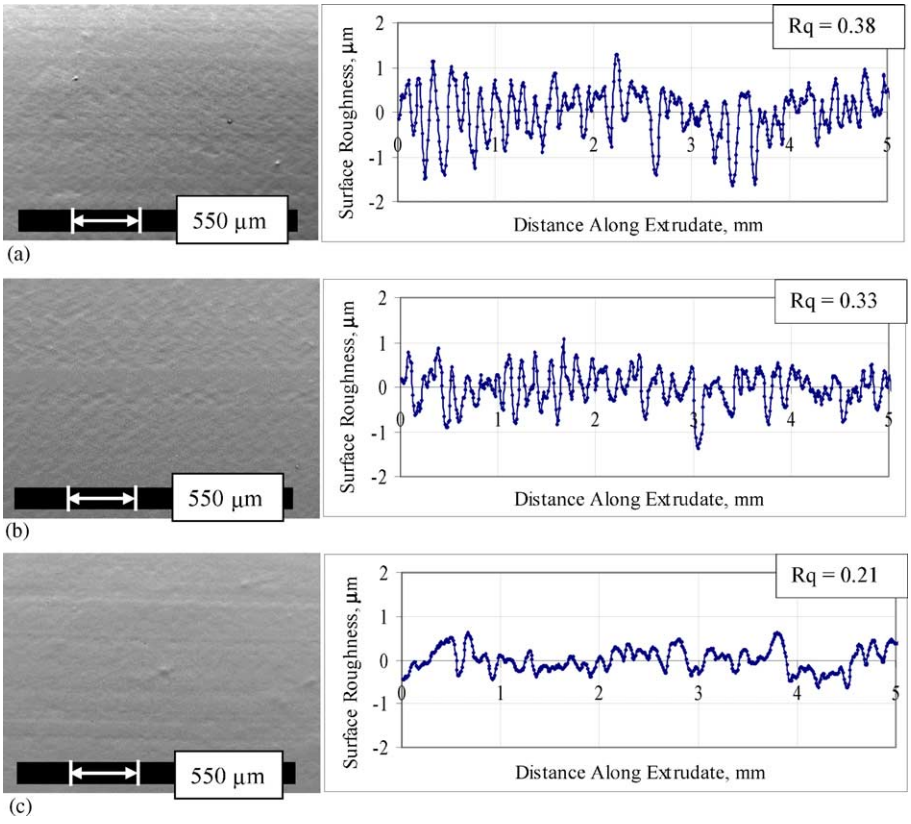

Fig. 5. SEM images and surface profilometry profiles with Rq values for extrudate surfaces of the LLDPE extruded at 0.6 rpm and 190 °C through dies (a) A, (b) B and (c) C.

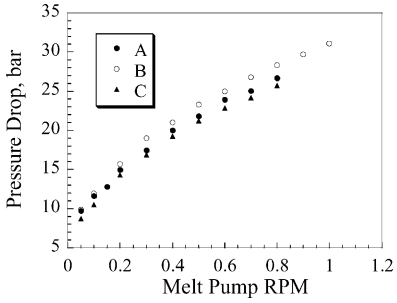

Fig. 6. Pressure drops across dies A–C for extrusion of the LLDPE at 190 °C at varying flow rates.

from the die at a sharp position (the corner of the die exit), with curved exit dies it is possible for the melt to separate at a wider range of positions. It is possible that this latter feature promotes the extrudate to emerge in a wavy formation. Furthermore, it could be conjectured that this also extends to cases of smaller scale. If the stability of the melt/wall separation point for 2 mm radiused exit dies generates waves with wavelengths of the order of centimetres (as was observed experimentally), it is not inconceivable that a sharp 90° exit could generate sharkskin waves of the order of microns. This could be one of the factors, in addition to the stress concentration, that are involved in the mechanism behind the sharkskin instability, as proposed by Dhori et al. [26–28].

4.1.5. Numerical simulation

In order to investigate the stresses in the melt at the die exit, simulations were carried out to observe the principal stress differences values along streamlines 50 μm from the die wall. The results are shown in Fig. 7. The plots show that there is a PSD peak at the die exit due to the abrupt change in boundary condition of the melt as it leaves the die. The results also show that with the delayed separation of the melt from the die exit, the PSD peak for die C is lower than that of die B, which in turn is lower than that of die A. This corresponds to the experimental result that the magnitude of sharkskin is lower for die C than die B, and lower for die B than die A.

4.1.6. Polymer material

The metallocene HDPE, which was found to exhibit significantly severer sharkskin than the LLDPE, was also used in extrusion experiments through dies A and C. As with the LLDPE, the HDPE birefringence stress field qualitatively showed a smaller stress concentration for die C as compared to die A. The extrusion pressure drops through die C were found to be at least 20% lower than through die A. SEM images of the resulting HDPE extrudate surfaces showed that while sharkskin was present for extrusion through both dies, the sharkskin magnitude through die C appeared to be much lower. This was quantified using surface profilometry measurements, which showed that the surface roughness of the extrudate from die C was reduced by 70% compared to the

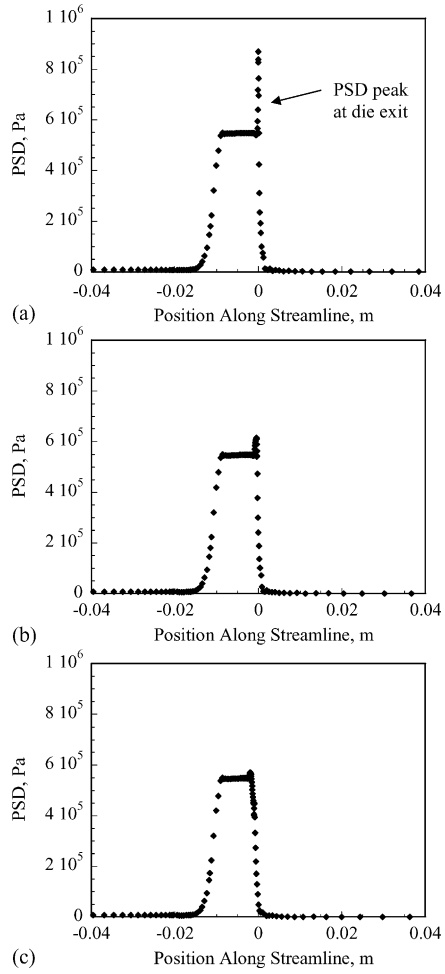

Fig. 7. PSD values along streamlines 50 μm from the die wall simulated in polyflow for the LLDPE at 190 °C through dies (a) A, (b) B and (c) C.

extrudate from die A. Die exit curvature was, thus shown to be a viable method of minimising sharkskin for both the LLDPE and the HDPE. A disadvantage of this method, however, is that it would not be suitable for applications where precision of the extrudate profile is of importance, since accuracy of the extrusion profile is not as high as for a sharp die exit. However, die exit curvature could be suitable for applications such as film production, where control of the extrusion profile could be compensated for by increased draw down.

4.2. The effect of die surface roughness

4.2.1. Stress field

In this set of experiments the die geometry was held constant and the surface roughness of the inside of the die wall varied. All exits were radiused to a 0.8 mm curvature. Fig. 8 shows the flow birefringence images captured for extrusion of LLDPE through dies D (most rough surface), E and F (least rough surface) at 0.05 rpm and 190 °C. In the parallel section of the die, the fringes and therefore the stresses are parallel to the die wall. Die F appears to have fewer fringes than dies D and E indicating that the stresses are lower in

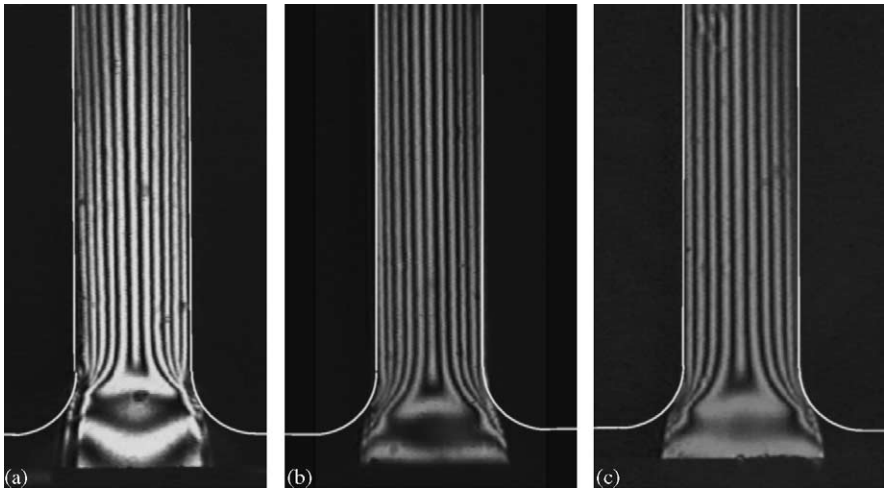

Fig. 8. Flow birefringence images for the LLDPE extruded at 0.05 rpm and 190 °C through dies (a) D, (b) E and (c) F.

the smoother dies. It can also be observed that the separation point of the melt from the die appears to be delayed further for die E as compared to die D and for die F as compared to die E. This last result is unexpected, as it was anticipated that the rougher the die surface, the longer the melt would grip to the die. Again the stress concentrations at the die exit are difficult to resolve.

4.2.2. Extrudate surface

SEM images of the LLDPE extrudate surfaces extruded at 0.8 rpm are shown in Fig. 9. This is a high flow rate, experimentally found to be within the sharkskin regime. Sharkskin can be seen on the extrudate surfaces obtained from all three dies. The onset of the sharkskin instability, as observed visually by SEM occurred at 0.4 rpm for die D ($\tau_w = 0.16$ MPa),

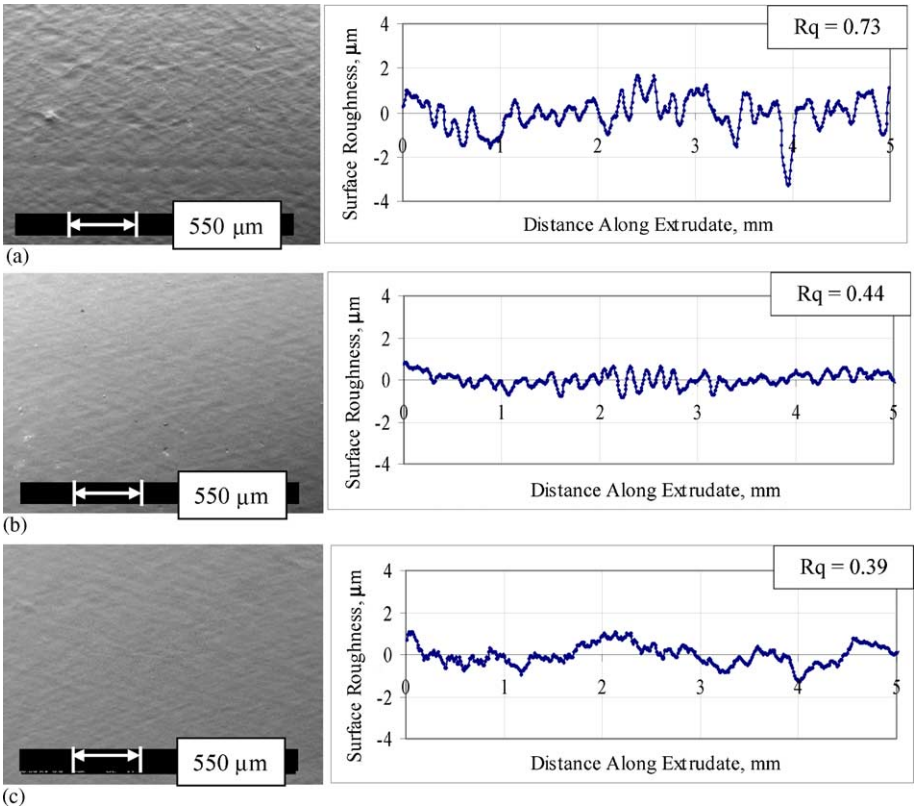

Fig. 9. SEM images and surface profilometry profiles with Rq values for extrudate surfaces of the LLDPE extruded at 0.8 rpm and 190 °C through dies (a) D, (b) E and (c) F.

at 0.6 rpm for die E (τ_w = 0.18 MPa) and at 0.7 rpm for die F (τ_w = 0.19 MPa).

The surface roughness of these extrudate surfaces was quantified using surface profilometry. The profiles obtained for LLDPE extrudate surfaces at 0.8 rpm are also shown in Fig. 9, together with the calculated Rq values. The results show that the magnitude of the sharkskin defect is reduced from die D to die E and from die E to die F. However, the scale of the sharkskin for all three dies is relatively small.

4.2.3. Comparison of pressure drop

A comparison of the pressure drops across dies D–F is shown in Fig. 10. A decrease in the pressure drop was found from die D to die E and from die E to die F. This decrease in pressure drop corresponds with the reduction in stress from die D to die F as observed in the birefringence images.

Decreasing die wall roughness was found to reduce sharkskin severity. A possible explanation for this is that there is an increase in partial wall slip with decreasing dies surface roughness. Slip at the wall will lower the wall stress, and thus also the extrusion pressure. Reduced extrusion pressure drops are observed for both dies E and F in comparison with die D. While the reduction in sharkskin severity could also be attributed to the delayed separation of the melt from the die, which appeared to occur for decreasing die surface roughness, the reduction in pressure drop and decrease in birefringence fringes would still suggest that a partial slip also occurs along the die surface.

4.2.4. Numerical simulation of partial slip

In order to investigate the effect of partial slip on stress concentrations at the die exit, numerical simulations were carried out with partial slip at a section of the die wall. The mesh used for this study is shown in Fig. 11. It was a parallel slit die with 90° entry and exit angles and a larger gap width of 3.8 mm. The geometry is different to those described previously as this set of simulations were carried out for a related program, further details of which can be found in [45]. The parameters used were for Dowlex at 190 °C. In order to simulate partial slip the simplest law available in polyflow was used, defined as:

$$f_s = -f_{slip} v_s \quad (1)$$

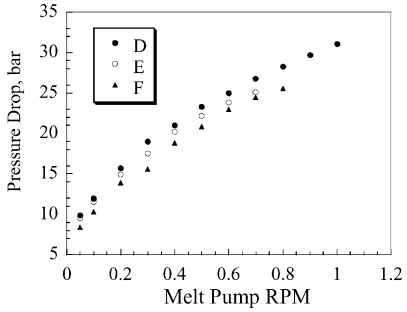

Fig. 10. Pressure drops across dies D–F for extrusion of the LLDPE at 190 °C at varying flow rates.

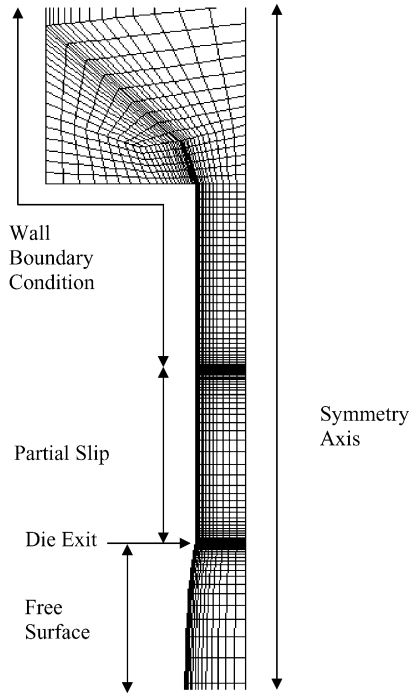

Fig. 11. Mesh used for numerical simulations of partial slip (2180 elements).

where f_s is the friction at the wall, v_s the velocity tangential to the wall and f_{slip} is the slip coefficient. The level of slip along a boundary was, therefore, varied by choosing different values for f_{slip}.

Fig. 12 shows a plot of the PSD in the melt along a streamline 50 μm from the die wall when there is no slip along the die wall. In this plot, a PSD peak is observed at the die entry corner and a larger one at the die exit. Fig. 13 shows the PSD along a streamline 50 μm from the die wall but this time with the presence of a certain level of partial slip ($f_{slip} = 1.5 \times 10^7$) along the die wall. The results show that with partial slip, although a PSD peak is introduced at the slip initiation point, both this peak and the die exit peak are smaller than for a die exit PSD peak without slip at the wall. A reduction in sharkskin would, therefore be expected for certain levels of partial slip. Further details and results of partial slip simulations are given in [45].

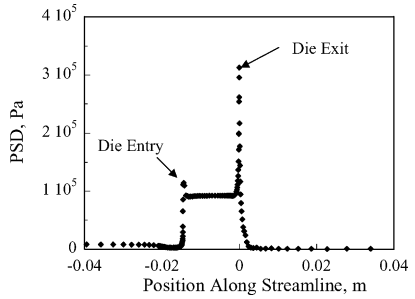

Fig. 12. PSD values simulated in polyflow for the LLDPE melt at 190 °C with no slip along the die wall along a streamline 50 μm from the die wall.

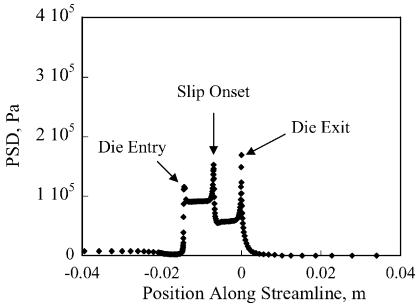

Fig. 13. PSD values simulated in polyflow with a partial level of slip ($f_{slip} = 1.5 \times 10^7$) along a streamline 50 μm from the die wall for LLDPE at 190 °C.

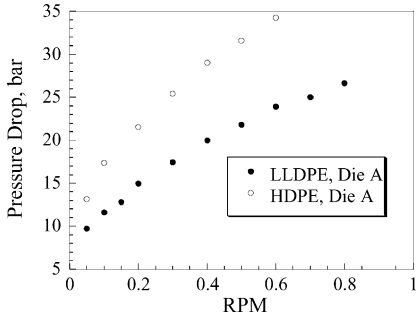

Fig. 15. Plot of extrusion pressure drop vs. melt gear pump speed for extrusion of the LLDPE and the HDPE through die A at 190 °C.

4.3. Comparison between LLDPE and HDPE

4.3.1. Stress field

The flow birefringence images for the LLDPE and the HDPE flowing through the conventional 90° exit die (die A) are shown in Fig. 14. The images show that for both polymers, the stresses in the die are parallel to the die wall and relax as the melt exits the die. The image for HDPE shows a larger number of fringes indicating that at these flow conditions stresses are higher in the die for the HDPE.

4.3.2. Comparison of pressure drop

The pressure drops for LLDPE and HDPE in die A are shown in Fig. 15. The HDPE pressure drops are significantly higher than those for the LLDPE.

4.3.3. Extrudate surface

SEM images of the LLDPE and HDPE extrudate surfaces from die A, at the moderately high flow rate of 0.6 rpm, and are shown in Fig. 16. The images show that the sharkskin on the HDPE surface is significantly severer than on the LLDPE surface. Both the amplitude and wavelength of the sharkskin are much larger. The sharkskin appears as three-dimensional waves across the surface of the extrudate. The surface profilometry results for the extrudates can also be seen in Fig. 16, which shows that the surface roughness of the HDPE is over 80 times higher than that of the LLDPE.

4.3.4. Numerical simulation

polyflow numerical simulations were carried out for the LLDPE and HDPE assuming no slip for both cases. The results showed no difference between the magnitudes of the exit stress concentrations for the two polymers. However, the flow birefringence in Section 4.3.1 clearly shows that the stresses in the HDPE are higher than LLDPE for the same volumetric flow rate. This suggests that the difference in the stresses observed between the LLDPE and the HDPE cannot be predicted by the parameters obtained from the rheological characterisation of the material alone (i.e. the spectrum parameters and the non-linear damping factor). It also appears that they are not due to a difference in viscosity, as characterisation results also show a similar apparent viscosity for the same shear rates. A possible explanation could be that the LLDPE exhibits partial slip along the die wall, whereas the HDPE does not. This has been shown by velocimetry measurements [46] and would account for the lower pressure drop and fewer birefringence fringes for LLDPE even

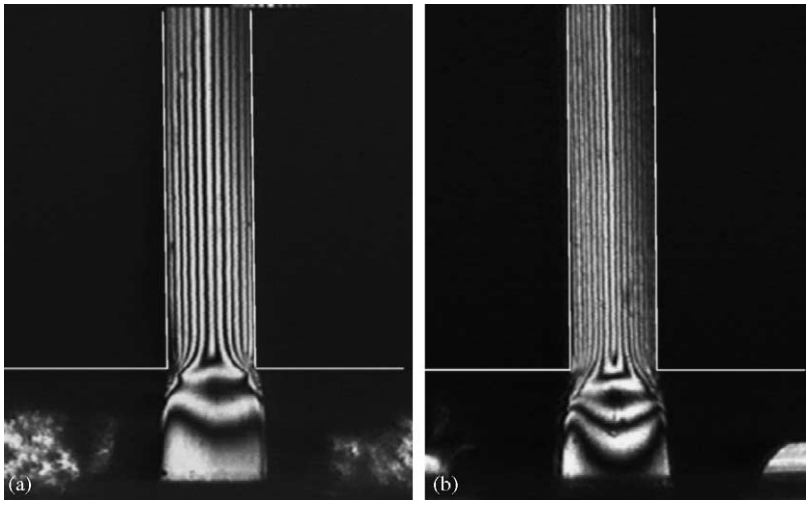

Fig. 14. Flow birefringence images for (a) LLDPE and (b) HDPE extruded at 0.05 rpm and 190 °C through die A.

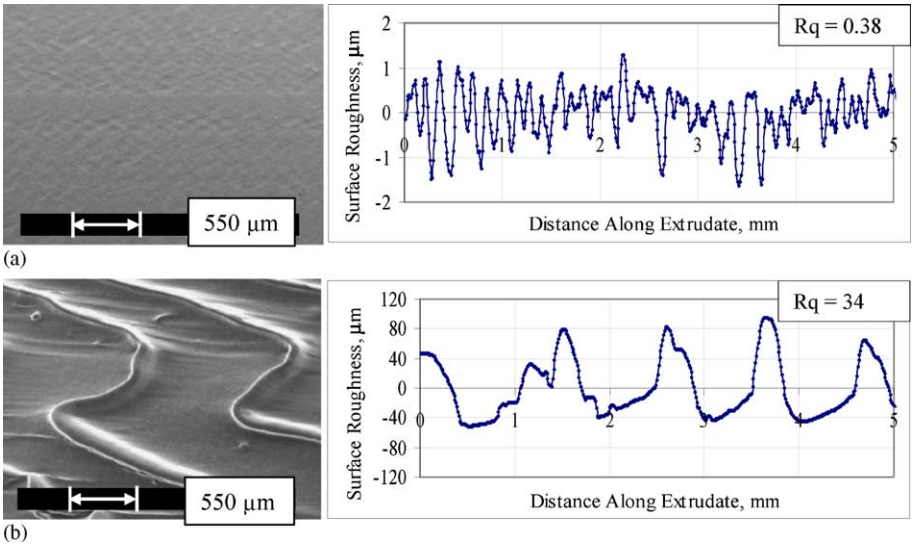

Fig. 16. SEM images and surface profilometry profiles with Rq values for extrudate surfaces of (a) LLDPE and (b) HDPE extruded at 0.6 rpm and 190 °C through die A (note ordinate scale difference).

though simulations predict that these should be the same for both polymers.

While the HDPE shows a much higher extrusion pressure drop and a correspondingly higher number of birefringence fringes for the same volumetric flow rate as the LLDPE, the LLDPE does not exhibit such severe sharkskin even for same pressure drop and number of birefringence fringes. There must be something other than the pressure drop and flow birefringence that accounts for the difference in the sharkskin severity between the two polymers. The other possible factors that could be responsible are discussed in the conclusions to this paper.

4.4. The effect of a fluoropolymer additive

In this section experiments that were carried out with the HDPE containing 1500 ppm of fluoropolymer as a polymer-processing additive are described. The preparation of the material is detailed in Section 2 of this paper. Rheological characterisation experiments showed that G', G'' and η^* for the HDPE were not modified by addition of the fluoropolymer. It was not possible to carry out flow birefringence for the HDPE with PPA as the fluoropolymer was opaque, and therefore did not allow penetration of light though the die.

4.4.1. Comparison of pressure drop

The pressure drops for pure HDPE and HDPE with PPA through die A at 190 °C are shown in Fig. 17. As expected, the pressure drops for the pure HDPE are significantly higher than those of the HDPE with PPA, indicating the presence of partial slip with the addition of the fluoropolymer.

4.4.2. Extrudate surface

SEM images of the pure HDPE and HDPE with PPA extrudate surfaces from die A at 0.6 rpm are shown in Fig. 18. The images show that sharkskin is completely eliminated from the surface of the HDPE with PPA. There appears to be microscopically small scratch marks at the side of the extrudate tape of the HDPE with PPA. However, this only appears on one side of the tape suggesting it was due to a small protrusion on the die wall. This extrudate also visually shows what look like very small bubbles on the extrudate surface. There is no explanation for these at present, but they appeared for all HDPE extrudates with the fluoropolymer as PPA. Surface profilometry results for the HDPE and the HDPE with PPA extruded at 0.6 rpm and 190 °C is also shown in Fig. 18. The surface roughness of the HDPE extrudate is over 55 times higher than the roughness of the HDPE with PPA. The PPA completely eliminated sharkskin in the HDPE for all flow rates studied in this paper.

The extrusion pressure drops suggest that the fluoropolymer imparts a slip boundary condition along the die wall. The level of slip imparted cannot be obtained using flow velocimetry techniques due to the opaque nature of the fluoropolymer additive. However, Stewart and Dealy [35] reported that for an optimised system, slip velocity is found to increase with in-

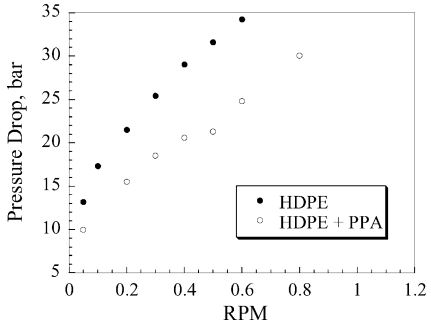

Fig. 17. Plot of extrusion pressure drop vs. melt gear pump speed for extrusion of the pure HDPE and the HDPE with PPA through die A at 190 °C.

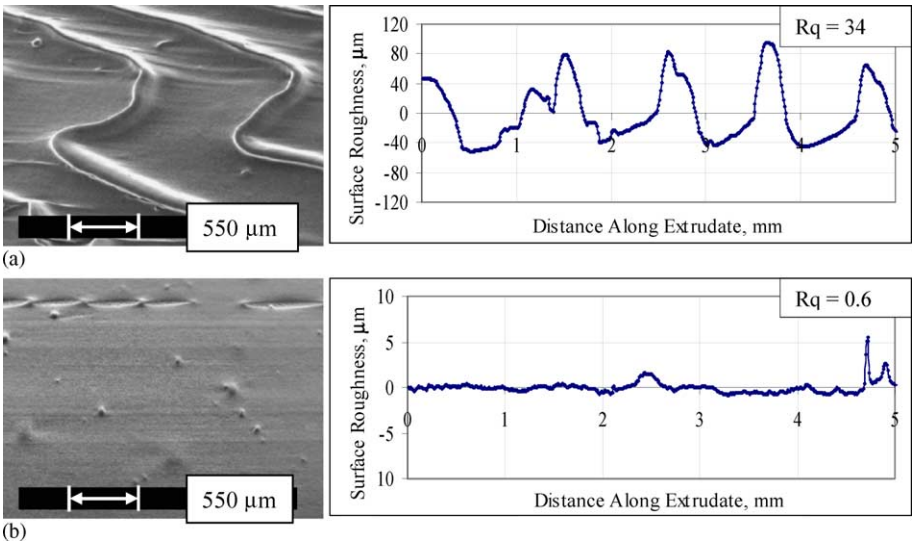

Fig. 18. SEM images and surface profilometry profiles with Rq values for extrudate surfaces of (a) HDPE and (b) HDPE + PPA extruded at 0.6 rpm and 190 °C through die A (note ordinate scale difference).

creasing fluoropolymer concentration up to about 500 ppm, while for higher fluoropolymer concentrations, the slip velocity remains practically constant. The fluoropolymer, thus eliminates the local die exit stress concentrations, and since the additive coats all surfaces, there are no additional stress concentrations elsewhere. Sharkskin is therefore completely eliminated.

5. Conclusions

Experimental results reported in this paper show that curvature of the die exit reduces sharkskin. Optical observations at the die exit show a delay in the separation point of the melt from the die. This delay in melt/wall separation for curved exit dies is believed to allow the stresses at the die exit to relax, and hence reduce the exit melt stress concentrations. Numerical simulations confirm that with the separations points experimentally observed for curved exit dies, there is a reduction in the stress concentration at the die exit. Flow birefringence exit fringe concentrations are also qualitatively observed to reduce with increasing die exit curvature. The number of fringes identified within the main die area, as well as the pressure drops, are not observed to change with die exit curvature. These results are consistent with those of Rutgers and Mackley [47] who found a reduction in sharkskin for a 0.5 mm radiused exit die. A further observation from curved exit dies is that with increased exit curvature, a wavy extrudate was obtained, possibly originating from the fact that with die exit curvature, the melt/wall separation point at the die exit is less well defined. It could be conjectured that at a micron scale, this instability of the melt/wall separation point can also promote the development of the sharkskin instability.

Reducing the roughness of the die surface has been experimentally found to reduce sharkskin. Using three progressively smoother dies led to a progressive reduction in the magnitude of sharkskin. This result is consistent with simulations of partial slip along the die wall, which show reduced stress concentrations for certain levels of slip. Partial slip is consistent with the reduced pressure drop and reduced number of birefringence fringes observed for the smoother dies. It is therefore possible that decreasing die surface roughness reduces sharkskin by allowing partial slip of the melt along the die wall, and thereby reducing the magnitude of the stress concentration at the die exit.

Different polymers show different levels of sharkskin for the same volumetric flow. The sharkskin on the metallocene HDPE was found to be significantly severer than on the LLDPE. At a given flow rate, higher pressure drops and more birefringence fringes were observed for the HDPE. However, this does not completely explain the difference in sharkskin severity between the two polymers, since for the same pressure drop and stress field, the sharkskin exhibited by Dowlex LLDPE is still significantly less pronounced. While it is clear that stress concentrations are a crucial factor for the development of the sharkskin instability, they cannot be the only factor. Issues that may also be involved include melt strength [12], the level of wall slip [20], the stability of the partial slip boundary condition [25] and the stability of the point of separation of the melt from the die exit [26–28].

A well-established way of reducing sharkskin is using a fluoropolymer additive (see, for example [20,22]) and experimental results reported in this paper confirm this. A fluoropolymer additive was found to dramatically eliminate sharkskin as well as reduce the extrusion pressure drop. This is consistent with simulations of partial slip, which predict a reduced pressure drop for extrusion with partial slip along

the die wall. Since the additive is deposited along the whole of the die surface, as well as the extruder screw and barrel [35], a stress concentration arises only at the die exit. The magnitude of this stress concentration is lower than that for a die with no slip, since the change in boundary condition from stick to partial slip is not as abrupt as a change from stick to full slip, as at the die exit. Additives are thus a very effective method for eliminating sharkskin.

In summary, the results presented in this paper support the model that sharkskin instabilities are a consequence of local melt stress concentrations. Techniques that reduce the magnitude of the stress concentration, for example die exit curvature (which allows the exit melt stresses to relax), decreasing die wall roughness (which is believed to allow a partial wall slip) and introduction of a polymer-processing additive (which also provides wall slip) have all been found to reduce the severity of the sharkskin instability. However, the fact that the metallocene HDPE shows significantly severer sharkskin than the LLDPE for the same extrusion pressure drop and stress field, indicates that stress concentrations alone are not the only factor of importance, but other issues such as melt strength, stability of the partial slip boundary condition or the melt/wall separation point must also contribute. Further work is required to determine the exact mechanism by which stress concentrations cause sharkskin, whether it is by melt rupture at or downstream of the die exit, whether it involves the wall slip boundary or die exit stability, or whether it involves another factor that has not yet been covered.

Acknowledgements

The authors would like to thank the EU for the funding of this project Postpone Polymer Processing Instabilities (3PI). They would also like to thank Prof. J.F. Agassant, Dr. B. Vergnes and Dr. O. Kulikov for useful discussions on the subject. Tony Burgess is thanked for his assistance obtaining the SEM photographs.

References

[1] C.J.S. Petrie, M.M. Denn, Instabilities in polymer processing, AIChE J. 22 (2) (1976) 209–236.
[2] M.M. Denn, Issues in viscoelastic fluid mechanics, Annu. Rev. Fluid Mech. 22 (1990) 13–34.
[3] R.G. Larson, Instabilities in viscoelastic flow, Rheol. Acta 31 (1992) 213–263.
[4] J.P. Tordella, in: F.R. Eirich (Ed.), Rheology, vol. 5, Academic Press, New York, 1969, p. 57.
[5] M.M. Denn, Surface-induced effects in polymer melt flow, in: P. Moldenaers, R. Keunings (Eds.), Theoretical and Applied Rheology, in: Proceeding of the Eleventh International Congress on Rheology, Elsevier, New York, 1992, pp. 45–49.
[6] S.Q. Wang, Molecular transitions at polymer/wall interfaces: origins of flow instabilities and wall slip, Adv. Polym. Sci. 138 (1999) 227–275.
[7] J.J. Benbow, P. Lamb, New aspects of melt fracture, S.P.E. Trans. 3 (1963) 7–17.
[8] R.H. Moynihan, D.G. Baird, R. Ramanathan, Additional observations on the surface melt fracture behaviour of LLDPE, J. Non-Newtonian Fluid Mech. 36 (1990) 255–263.
[9] F.N. Cogswell, Stretching flow instabilities at the exits of extrusion dies, J. Non-Newtonian Fluid Mech. 2 (1977) 37–47.
[10] P. Beaufils, B. Vergnes, J.F. Agassant, Characterization of the sharkskin defect and its development with the flow conditions, Int. Polym. Proc. 4 (2) (1989) 78–84.
[11] N. El Kissi, J.M. Piau, Adhesion of linear low density polyethylene for flow regimes with sharkskin, J. Rheol. 38 (5) (1994) 1447–1463.
[12] R.P.G. Rutgers, M.R. Mackley, The correlation of experimental surface extrusion instabilities with numerically predicted exit surface stress concentrations and melt strength for linear low-density polyethylene, J. Rheol. 44 (6) (2000) 1319–1334.
[13] N. Bergem, Visualization studies of polymer melt flow anomalies in extruders, in: Proceeding of Seventh International Congress on Rheology, Gothenberg, 1976, p. 50.
[14] S.J. Kurtz, Die geometry solutions to sharkskin melt fracture in advances in rheology, in: Nineth International Congress on Rheology, Mexico, 1984, pp. 399–407.
[15] Y.W. Inn, R.J. Fischer, M.T. Shaw, Visual observation of development of sharkskin melt fracture in polybutadiene extrusion, Rheol. Acta 37 (1998) 573–582.
[16] F. Legrand, J.M. Piau, Spatially resolved stress birefringence and flow visualization in the flow instabilities of a polydimethylsiloxane extruded though a slit die, J. Non-Newtonian Fluid Mech. 77 (1998) 123–150.
[17] A.V. Ramamurthy, Wall slip in viscous fluids and influence of materials of construction, J. Rheol. 30 (2) (1986) 337–357.
[18] M. Mooney, Explicit formulas for slip and fluidity, J. Rheol. 2 (1931) 210–222.
[19] D.S. Kalika, M.M. Denn, Wall slip and extrudate distortion in linear low-density polyethylene, J. Rheol. 31 (1987) 815–834.
[20] K.B. Migler, Y. Son, F. Qiao, K. Flynn, Extensional deformation, cohesive failure, and boundary conditions during sharkskin melt fracture, J. Rheol. 46 (2) (2002) 383–400.
[21] X. Yang, H. Ishida, S.Q. Wang, Wall slip and absence of interfacial flow instabilities in capillary flow of various polymer melts, J. Rheol. 42 (1) (1998) 63–80.
[22] S.Q. Wang, P.A. Drda, Molecular instabilities in capillary flow of polymer melts: interfacial stick-slip transition, wall slip and extrudate distortion, Macromol. Chem. Phys. 198 (1997) 673–701.
[23] J.R. Barone, N. Plucktaveesak, S.Q. Wang, Interfacial molecular instability mechanism for sharkskin phenomenon in capillary extrusion of linear polyethylenes, J. Rheol. 42 (4) (1998) 813–832.
[24] S.Q. Wang, P.A. Drda, Y.W. Inn, Exploring molecular origins of sharkskin, partial slip, and slope change in flow curves of linear low-density polyethylene, J. Rheol. 40 (5) (1996) 875–898.
[25] J. Molenaar, R.J. Koopmans, Modeling polymer melt-flow instabilities, J. Rheol. 38 (1994) 99–109.
[26] P.K. Dhori, J.C. Slattery, Common line motion I: implications of entropy inequality, J. Non-Newtonian Fluid Mech. 71 (1997) 197–213.
[27] P.K. Dhori, A.J. Giacomin, J.C. Slattery, Common line motion II: sliding plate rheometry, J. Non-Newtonian Fluid Mech. 71 (1997) 215–229.
[28] P.K. Dhori, R.S. Jeyaseelan, A.J. Giacomin, J.C. Slattery, Common line motion III: implications in polymer extrusion, J. Non-Newtonian Fluid Mech. 71 (1997) 231–243.
[29] D.D. Joseph, Y.J. Liu, Letter to the editor: steep wave fronts on extrudates of polymer melts and solutions, J. Rheol. 40 (1996) 317–319.
[30] D.D. Joseph, Steep wave fronts on extrudates of polymer melts and solutions: lubrication layers and boundary lubrication, J. Non-Newtonian Fluid Mech. 70 (1997) 187–203.

[31] J. Barone, S.Q. Wang, Flow birefringence study of sharkskin and stress relaxation in polybutadiene melts, Rheol. Acta 38 (1999) 404–414.
[32] B. Tremblay, Sharkskin defects of polymer melts: the role of cohesion and adhesion, J. Rheol. 35 (6) (1991) 985–998.
[33] D.E. Priester, C.W. Stewart, New Processing Additives for Polyolefins Minimize Formulation Interactions, SPE ANTEC, Detroit, 1992, pp. 2024–2028.
[34] C.W. Stewart, Wall slip in the extrusion of linear polyolefins, J. Rheol. 37 (3) (1993) 499–513.
[35] C.W. Stewart, J.M. Dealy, Technical note: new information on the mechanism of action of the adhesion promoter reported in wall slip of molten high density polyethylene, J. Rheol. 35 (1991) 497;
C.W. Stewart, J.M. Dealy, Technical note: new information on the mechanism of action of the adhesion promoter reported in wall slip of molten high density polyethylene, J. Rheol. 36 (5) (1992) 967–969.
[36] F. Yip, S.G. Hatzikiriakos, T.M. Clere, A new processing aid for the extrusion of polyolefins, J. Vinyl Addit. Technol. 6 (2) (2000) 113–118.
[37] E.E. Rosenbaum, S.K. Randa, S.G. Hatzikiriakos, C.W. Stewart, D.L. Henry, M. Buckmaster, Boron nitride as a processing aid for the extrusion of polyolefins and fluoropolymers, Polym. Eng. Sci. 40 (1) (2000) 179–190.
[38] J.M. Piau, N. El Kissi, F. Toussaint, A. Mezghani, Distortions of polymer melt extrudates and their elimination using slippery surfaces, Rheol. Acta 34 (1995) 40–57.
[39] S.G. Hatzikiriakos, J.M. Dealy, Effects of interfacial conditions on wall slip and sharkskin melt fracture of HDPE, Int. Pol. Proc. 8 (1993) 30–35.
[40] O. Kulikov, K. Hornung, A simple way to suppress surface defects in the processing of polyethylene, in: Proceedings of Twelfth International Conference of Deformation, Yield and Fracture of Polymers, Cambridge, 2003, pp. 411–414.
[41] D.R. Arda, The sharkskin extrusion instability and its minimisation in polyethylene processing, Ph.D. Thesis, Cambridge, 2003.
[42] G.G. Lipscomb, R. Keunings, M.M. Denn, Implications of boundary singularities in complex geometries, J. Non-Newtonian Fluid Mech. 24 (1) (1987) 85–96.
[43] M. Renardy, Current issues in non-newtonian flows: a mathematical perspective, J. Non-Newtonian Fluid Mech. 90 (2–3) (2000) 243–259.
[44] C. Venet, B. Vergnes, Experimental characterization of sharkskin in polyethylenes, J. Rheol. 41 (4) (1997) 873–892.
[45] D.R. Arda, M.R. Mackley, Sharkskin instabilities and the effect of slip from gas-assisted extrusion, Submitted to Rheol. Acta, March 2004.
[46] H. Munstedt, A. Merten, A personal communication, 2004.
[47] R.P.G. Rutgers, M.R. Mackley, The effect of channel geometry and wall boundary conditions on the formation of extrusion surface instabilities for LLDPE, J. Non-Newtonian Fluid Mech. 98 (2001) 185–199.